EFFECT OF PULSING PARAMETERS ON LASER ABLATIVE CLEANING OF COPPER OXIDES

Paper # M602

Jie Zhang, Youneng Wang, Peng Cheng, Y. Lawrence Yao

Department of Mechanical Engineering, Columbia University, New York, NY 10027, USA

Abstract

The characteristics of copper oxides removal are comparably investigated under different pulsing strategies. A two-dimensional model is utilized to numerically simulate the laser ablative cleaning process. In the model, property discontinuity and Stephan and kinetic boundary condition are taken into account, and the moving phase-interface in the material is evaluated with the enthalpy method. Experiments are carried out on copper samples having different oxide layer thickness. The copper oxide layer thickness determined by ellipsometer, and the chemical constituents of the copper oxide layer determined via X-ray photoelectron spectroscopy (XPS), are incorporated into this numerical model. Under the single- pulse irradiation strategy, a higher laser intensity threshold is determined by the model based on the criterion of removing the oxide film as much as possible without damaging the substrate. Under the multi-pulse irradiation strategy, a lower threshold is employed to remove the oxide layer while the appropriate pulse number under different laser intensity and different laser pulse repetition rate are the key issues investigated. Reasonable agreement is obtained between the experimental and simulated results.

Introduction

How to remove contaminations and oxides from surfaces has been an active research topic for many years in that clean surfaces are extremely vital in the fabrication of semiconductor [1], microelectronic device, integrated circuits, and even in the maintenance of the nuclear reactor [2]. At present, the wet chemical flux and ultrasonic/megasonic are the most widely used methods to clean surfaces. However, the former is not environmentally benign, and the latter can not produce sufficient cleaning forces in some cases. The disadvantages of these methods stimulated researchers to seek alternative cleaning methods.

Laser cleaning, using short pulsed laser irradiation to clean surfaces, has emerged as a promising method because of its prominent advantages such as selectivity, controllability, and flexibility. Moreover, laser cleaning is easy to be automated and integrated into the production line. Besides being explored for the use in art restoration, this environment-friendly technique is also utilized to remove nano-scale particles from semiconductor surfaces [3], to strip painting or oxides layer from metals or semiconductors [4-6]. Furthermore, laser cleaning can be integrated into other cleaning methods to significantly enhance the cleaning efficiency [7].

Laser removal of thin contamination layer from the substrate mainly involves several competing mechanisms, such as ablation, photospallation, and acoustic excitation due to rapid thermal expansion [8]. For the transparent layer, such as silicon dioxide, the acoustic pulse induced by the absorption of the laser energy at the substrate/layer interface is the main power to remove the thin layer [9]. For the opaque layer, if the applied laser intensity is too low to melt the layer, the thermal stress due to the very quickly heating of laser pulse is responsible for the layer removal [10]. Generally, the relatively high laser intensity is used to remove the contamination layer based on the working mechanism of laser ablation.

Copper is the most widely utilized metal in the fabrication of printed circuit board and integrated circuits due to its excellent electrical conductivity and less electromigration. However, the disadvantages of Cu are that it is easy to be naturally oxidized and its oxidation is not self-limiting, which imposes a significantly negative effect on the work performance of the entire system. Therefore, the laser removal of copper oxide dominated by the ablation mechanism has drawn the investigation interests.

Wesner et al. explored the possibility of laser removal of the copper oxide, and monitored the cleaning results with X-ray Photoelectron Spectroscopy (XPS) spectrum analysis [11]. Yonezawa et al. found that the results of the copper oxides removal were dependent

on the applied laser intensity. And, the morphology change was possibly due to the explosion or transport of molten materials [12]. Kerrns et al. investigated the effect of wavelength on the laser fluence threshold for laser removing of copper oxide as well as the material removal mechanisms at different laser wavelengths [13].

Pulse parameters play a key role in the success of the laser cleaning, namely removing the contaminations or oxides without any damage to the underlying substrate. Wesner et al. found that a large number of pulses at a low fluence could achieve the cleaning quality similar to that produced by a small number of pulses at a high fluence. And, the thermal accumulation might limit the number of pulses and the fluence [11]. However, this area is far from fully understood, especially in the analytical sense. Lee et al. proposed a one-dimensional heat conduction model to numerically determine the laser fluence threshold for the cleaning of copper oxide and investigate the cleaning mechanism at different wavelengths based on this model [14]. However, this model was inaccurate due to the neglect of many basic phenomena of laser ablation. Lee et al. formulated a one-dimensional heat flow model incorporating melting and vaporization to seek the optimal processing conditions [15]. In this model, property discontinuity at the Knudsen layer and the kinetic phase boundary were not considered.

In this paper, a two-dimensional mathematic model is utilized to more accurately simulate laser cleaning under the ablation mechanism. Under the single-pulse strategy, the laser intensity threshold is determined by experiments and simulations, respectively. Under the multi-pulse strategy, a lower threshold is employed to remove the oxide layer. The influence of laser intensity and repetition rate on pulse number is studied via experiments and numerical simulation.

Experiment Conditions and Measurement

Experiment Conditions

Laser irradiation experiments are preformed using a Q-switched Nd:YAG laser with the wavelength of 355 nm and the pulse duration of 50 ns. The laser beam intensity has a Gaussian distribution. The laser intensity irradiated on the sample surface can be adjusted through changing the distance between the sample and the focusing lens. The repetition rates of 1 kHz and 2 kHz are used, the beam quality parameter M^2 is 1.49 and the minimal beam diameter is 12 μm.

The laser system is composed of the Nd:YAG laser source, CCD camera, TV monitor, sample stages and control system. The laser cleaning experiments are carried out in open air. During the experiments, a gas jet flows onto the sample to prevent the plasma formed by laser ablation from getting onto the focusing lens.

The samples are pure copper (15×15 mm, 0.8 mm thick), which are mechanically polished. They are divided into two groups and baked in an oven at 250˚C for 30 minutes and 45 minutes, respectively. After baking, the copper oxide layers with two different thicknesses are formed to allow the study of the effect of oxide layer thickness on laser intensity threshold.

Material Characterization

The thickness of copper oxide layer is measured with the Beaglehole Spectroscopic ellipsometer. The ellipsometer is based on the measurement of the change in the state of light polarization caused by its interaction with the sample, defined with two quantities Δ and ψ, to characterize thin films [16]. Film thickness and optical constants can be deduced from Δ and ψ using a model of optical physics. In this paper, ellipsometry measurements are performed at the Brewster angle of 68 degree. The wavelength of the incident light varies from 300 nm to 800 nm with a step of 4 nm. The software of Filmwizard is employed to deduce the results.

X-ray Photoelectron Spectroscopy (XPS) (PHI 550 ESCA XPS/ISS Spectrometer) is used to analyze the chemical constituents of pre and post-cleaned copper oxide layers. XPS uses a soft X-ray source (Alk_α and Mgk_α) to ionize electrons from the surface of a solid sample. The binding energies of these electrons are measured and are characteristic of the elements and the associated chemical bonds (chemical state) in the top few atomic layers of the material [17]. Usually, the measurement depth of XPS is around 10-30 nm.

The mechanism of the space-charge oxidation processes is helpful to verify that the copper oxides formed at 250˚C are composed of cupric oxide (CuO) and cuprous oxide (Cu_2O) and their distributions vary along the thickness direction [18]. Due to the large electron affinity of the chemisorbed oxygen, electrons are withdrawn from the oxide to form ions (i.g. O^-), additional holes are created in a p-type conducting oxide of Cu_2O, which results in that the cations concentration is higher than the vacancy concentration. Hence, the space-charge field is setup, counteracting the chemical concentration gradient. The chemisorption of oxygen on the interface of oxide is written as:

$$\frac{1}{2}O_2^{(g)} + 2 \otimes (Cu) \leftrightarrow Cu_2O + 2Cu \oplus \quad (1)$$

When the space-charge field is in equilibrium with the chemical concentration gradient, the growth of an oxide layer will cease. Before that, with the thickening of oxide layer, more and more free electrons are thermally emitted and enter the space-charge layer. Rapid field transport of copper ions through vacancies keeps the stationary surface concentration of the oxygen low. Then, CuO is generated starting from the interface of oxygen and Cu_2O. A thin layer of Cu_2O always exists on the copper substrate

Images of pre and post-cleaned copper oxide layers are obtained using Scanning Electron Microscopy (JEOL). Atomic Force Microscopy (AFM Dimension 3000) is employed to measure the crater generated by the laser irradiation on the sample.

Two-Dimensional Laser Ablative Cleaning Model

During the laser ablative cleaning, the copper oxides are irradiated by the short laser pulse with the extremely high intensity, and thus experience fast melting and intensive evaporation. The traditionally used heat conduction model has no capability of reflecting this complex laser-solid interaction process. In addition, the laser beam diameter used for the experiment in this paper is 20 to 100 μm. Although it is larger than the oxide thickness, which usually is a few microns, and the thermal diffusion distance of $d = 2\sqrt{\alpha\tau} = 2.03\mu m$, where α is thermal diffusivity of the copper oxides and τ is the pulse width of 50 ns in this case, it is desirable to use a two-dimensional model to analyze the thermal field in the material more realistically.

Zhang et al. developed a two-dimensional model to describe the laser ablation of copper [19]. In fact, laser ablative cleaning is based on the ablation of oxide layer without damaging the substrate. However, this model of laser ablation can not be directly used to delineate the ablative cleaning without the necessary modifications.

The laser ablative cleaning model developed in this paper assumes that the target has a two-layer structure including copper oxides and copper, shown in Fig. 1. As mentioned before, the thickness of copper oxide layer is determined using the ellipsometry. Along the thickness direction, the distribution of CuO and Cu_2O is determined through XPS spectrum analysis of the copper sample gradually etched away. Within the range of copper oxides and copper, the corresponding material properties are used [20,21].

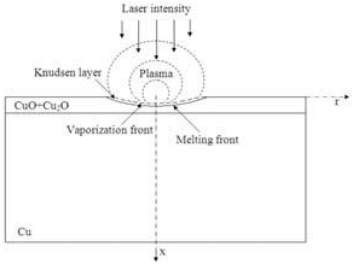

Fig. 1 Schematic of 2-D laser ablative cleaning model

The laser intensity absorbed by the sample is $Q = C(1-Rl)I\exp\left[-(r/b)^2\right]$, where C is the plasma correction coefficient [22], I is the laser intensity, b is the laser beam radius, the reflectivity of $Rl = \frac{(n-1)^2 + k^2}{(n+1)^2 + k^2}$, where n and k are indexes of refraction and extinction coefficient, respectively. At the wavelength of 355 nm, Cu has the indexes of refraction of 1.34, CuO 2.24, and Cu_2O 2.4. And, the extinction coefficient of Cu is 1.93, CuO 1.03, and Cu_2O 1.44 [23].

The model is briefly summarized as follows. It is assumed that the movement of molten material and heat loss from the surface are negligible. The heat conduction in the solid is described as

$$\frac{\partial T}{\partial t} - \frac{\partial T}{\partial x} - r\frac{\partial T}{\partial r} = \frac{1}{\rho_0 c_p}\left[k\frac{\partial^2 T}{\partial z^2} + r\frac{\partial}{\partial r}(kr\frac{\partial T}{\partial r}) - \frac{\partial Q}{\partial z}\right] \quad (2)$$

where t is the time, x and r are the coordinates along the thickness and radial direction, respectively, ρ_0 is the density of solid, c_p is the specific heat, and k is the heat conductivity.

At the vapor-liquid interface, the Stephan boundary condition is considered as [24]

$$Q + k\left(\frac{\partial T}{\partial x} + r\frac{\partial T}{\partial r}\right) + \rho_l v_i L_v - \rho_v v_v\left(c_p T_i + E_v\right) = 0 \quad (3)$$

where the gas energy $E_v = \frac{RT_v}{(\gamma-1)M_v} + \frac{1}{2}v_v^2$ includes the internal energy and kinetic energy. The subscripts l, v and i denote liquid phase, vapor phase and vapor-liquid interface, respectively. R is the universal gas constant, v is the velocity, L_v is the latent heat of vaporization, M_v is the molecular mass, and γ is the specific ratio.

The property discontinuity across Kudsen layer is described as [25]

$$\frac{T_{vi}}{T_{li}} = \left[\sqrt{1 + \pi \left(\frac{m}{2} \frac{\gamma - 1}{\gamma + 1} \right)^2} - \sqrt{\pi} \frac{m}{2} \frac{\gamma - 1}{\gamma + 1} \right]^2$$

$$\frac{\rho_{vi}}{\rho_{li}} = \sqrt{\frac{T_{li}}{T_{vi}}} \left[\left(m^2 + \frac{1}{2} \right) e^{m^2} erfc(m) - \frac{m}{\sqrt{\pi}} \right] + \frac{1}{2} \frac{T_{li}}{T_{vi}} \left[1 - \sqrt{\pi} m e^{m^2} erfc(m) \right]$$

$$e^{m^2} erfc(m) \approx 0.34802a - 0.09588a^2 + 0.74786a^3$$

$$a = 1/(1 + 0.47407m) \qquad m = \frac{V_{vi}}{\sqrt{2RT_{vi} / Ma_v}} \qquad (4)$$

where *vi* and *li* denote the value of the vapor and liquid adjacent to the Knudsen layer, respectively. Ma_v is the vapor Mach number, and *erfc(m)* the complementary error function. The gas velocity is obtained from mass conservation, such as $\rho_l v_i = \rho_v (v_i + v_v)$. The enthalpy method is applied to trace the interface of solid and liquid phase [26].

The control-volume method is adopted to solve the above coupled governing equations. According to the node temperature, the different phases of material are determined. In this paper, the evaporation temperature of CuO, Cu_2O and Cu is 2073 K, 2073 K and 2833 K, respectively. The melting temperature of CuO, Cu_2O and Cu is 1609 K, 1515 K and 1356 K, respectively [20,21]. The heat loss at the top surface and the movement of molten material are assumed to be negligible.

Results and Discussions

Copper Oxide Layer Characterization

Fig. 2 shows SEM images of cross-sections of two samples. It can be observed that the sample oxidized for 45 minutes has the oxide layer thicker than that of the sample oxidized for 30 min. This phenomenon is consistent with the conclusion that the oxide layer thickness is proportional to the oxidation temperature and time [18]. The thickness of oxide layer is also measured with the ellipsometer. The oxide layer thickness is about 1 μm and 2.5 μm for the samples oxidized for 30 min and 45 min, respectively.

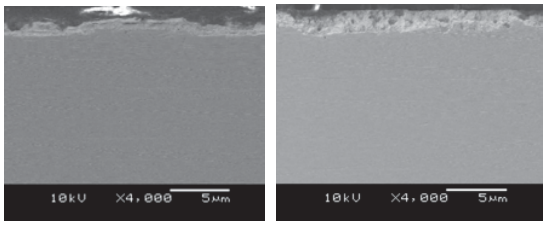

(a) (b)

Fig. 2 SEM images of the cross-section of Cu samples (a) oxidized for 30min (b) oxidized for 45min

The chemical distribution of copper oxides along the thickness direction is investigated with XPS analysis. These two samples having different oxide layer thickness are etched by 9% Hydrogen Chloride for 2 s in the 1 μm case and 5 s in the 2.5 μm case, respectively. In both cases, the time increment is 1 s. The oxide layer thickness of the etched sample is assumed to be inversely proportional to the etching time.

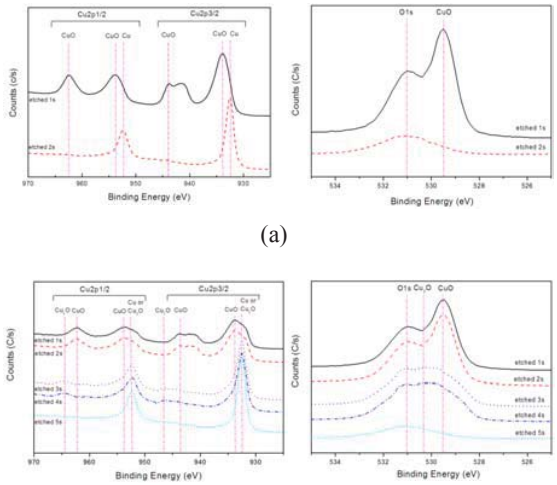

(a)

(b)

Fig. 3 XPS spectra of etched samples (a) oxidized for 30min (b) oxidized for 45min

The Cu 2p and O 1s XPS spectra of etched samples having 1 μm and 2.5 μm thick oxide layers are presented in Fig. 3 (a) and (b), respectively. The binding energy of Cu 2p and O 1s associated with CuO and Cu_2O are listed in Table 1. In Fig. 3 (a), the spectrum after etching for 1 s displays a Cu $2p_{3/2}$ peak at 934.5 eV corresponding to CuO, a shake-up satellite peak at about 9 eV higher than the $2p_{3/2}$ peak, and the peak above 950 eV arising from spin-orbit coupling [27]. This shows only CuO exists on the surface after 1 s etching. In the spectrum after etching for 2 s, the Cu $2p_{3/2}$ peak is located at 932.4 eV, which corresponds to Cu or Cu_2O. Cu_2O, however, is ruled out based on two facts: no Cu 2p satellite peak associated with Cu_2O,

and the O 1s peak at 531 eV without any shift caused by Cu_2O. This means there are no copper oxides on the surface after 2 s etching. In Fig. 3 (b), the spectra after etching for 1 s and 2 s show CuO still exists after 1 s and 2 s etching. In the spectra after 3 and 4 s, the Cu $2p_{3/2}$ peak is located at 932.4 eV again. However, the satellite peak associated with Cu_2O at 946.5 eV denotes the appearance of Cu_2O. It can be verified with O 1s spectrum. The O 1s peak shifts about 0.7 eV to a lower binding energy mainly due to the presence of Cu_2O. The last spectrum (after etching for 5 s) shows no existence of copper oxides.

Table 1 XPS data for copper oxides

XPS Cu $2p_{3/2}$	932.4 eV (Cu)	932.4 eV (Cu_2O)	934.5 eV (CuO)
XPS Cu $2p_{1/2}$	952.2 eV (Cu)	952.2 eV (Cu_2O)	954.3 eV (CuO)
XPS O 1s	531 eV (O)	530.3 eV (Cu_2O)	529.5 eV (CuO)

Suppose that the etching rates of CuO and Cu_2O with HCl are identical. According to XPS analysis of etched copper oxide layer, it can be deduced that CuO layer is above Cu_2O layer. For simplicity without losing generality, it is assumed that the top half of the layer is CuO and the bottom half is Cu_2O considering the oxidation temperature used in this paper is 250°C. This assumption is consistent with the work done by Haugsurd [28], in which he proposed that the CuO layer was around 70% of the total oxide thickness if the copper was oxidized at 500°C. CuO layer thickness decreased with the decrease of oxidation temperature according to [18]. The assumed distribution of CuO and Cu_2O in the thickness direction is integrated into the 2-D laser ablative cleaning model.

Single-pulse Irradiation Strategy

Under the single-pulse irradiation strategy, the aim is to remove the oxide layer as complete as possible in a single pulse without damaging the substrate.

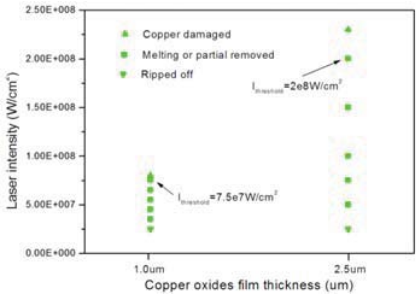

Fig. 4 Effects of laser intensity on the removal of copper oxides layers with different thickness

Experiment Fig. 4 presents the removal results of copper oxide layers with different laser intensity levels. For the sample with 1 μm thick copper oxide, the intensity of 2.5×10^7 W/cm^2 makes the oxide film ripped off without melting. This is possibly due to the shock wave generated by the quick thermal expansion of the material induced by the laser pulse. When the intensity rises to 3.7×10^7 W/cm^2, the copper oxide begins to melt. If the intensity reaches 8×10^7 W/cm^2, the substrate of copper begins to melt. Accordingly, the laser intensity threshold is determined as 7.5×10^7 W/cm^2. For the sample with 2.5 μm thick copper oxide, the similar results are obtained with the corresponding intensity threshold of 2×10^8 W/cm^2. It is clearly shown in Fig. 4 that the laser intensity threshold increases with the thickness of oxide layer.

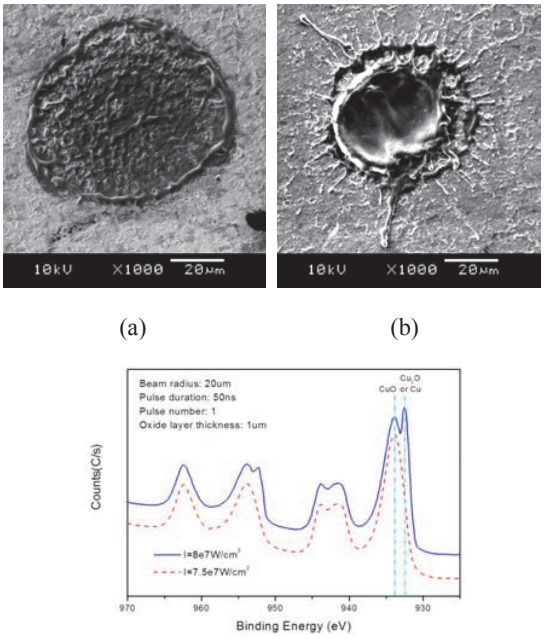

Fig. 5 SEM images of the samples irradiated by different laser intensity and the corresponding XPS spectra (a) 7.5×10^7W/cm^2 (b) 8×10^7W/cm^2 (c) XPS spectrum

The SEM images shown in Fig. 5 are the surface of the sample with 1 μm thick copper oxide irradiated by two laser intensity levels. It can be seen that the copper oxide is not totally removed by one pulse with the intensity of 7.5×10^7 W/cm^2. However, a little higher intensity leads to the damage of substrate. This indicates that it is difficult to experimentally determine a safe laser intensity threshold under this strategy.

XPS spectra shown in Fig. 5c are aimed at further confirming the cleaning results shown in Fig. 5a and 5b. The sample is irradiated by a matrix of 4×15 spots with the spacing of 200 μm to improve the quality of the XPS signal since the detected area of XPS is around 1mm^2. For 7.5×10^7 W/cm^2, the Cu 2p$_{3/2}$ main peak is at 934.5 eV, corresponding to CuO. And, the satellite line of CuO also appears. This means the pulse at this intensity threshold does not remove the copper oxide completely and not damage the copper substrate. For 8×10^7 W/cm^2, the XPS spectrum has a Cu 2p$_{3/2}$ peak at 932.4 eV with a shoulder at 934.5 eV, which corresponds to Cu and/or Cu_2O and CuO, respectively. Cu is determined because the satellites of Cu_2O do not exist. All of satellite lines are related to CuO. Evidently, the copper substrate is exposed due to the removal of copper oxide.

Model Prediction and Comparison The experimentally determined intensity thresholds are applied into the two-dimensional laser ablative cleaning model. The experimental and simulated results of crate depths and widths are listed in Table 2. The simulation slightly overestimates the ablation effects perhaps due to the insufficient consideration about plasma absorption of laser intensity and the neglect of the heat loss at the surface in 2-D cleaning model. The overestimate is beneficial to safe cleaning.

Table 2 Experimental and simulated depths and widths of the craters generated by laser intensity threshold

Oxide layer thickness	1 μm		2.5 μm	
Intensity threshold	7.5 ×10^7 W/cm^2		2 ×10^8 W/cm^2	
	Exp.	Sim.	Exp.	Sim.
Depth (μm)	0.954±0.1	1.04	2.48±0.15	2.58
Width (μm)	45±1.2	48	53±2	60

On determining the intensity threshold with 2-D laser ablative cleaning model, the intensity which makes the temperature of Cu surface 30 K below 1356 K (Cu's melting point) at the end of the laser pulse is regarded as the intensity threshold. According to this criterion, the intensity threshold is determined as $7\times10^7 W/cm^2$ and $1.7\times10^8 W/cm^2$ for samples with 1 μm and 2.5 μm thick oxide layer, respectively. Obviously, the thresholds determined by this model again slightly overestimate experimental results for the reason stated above. Fig. 6 shows the craters generated by laser intensity thresholds determined by the 2-D cleaning model. There is a thin layer of copper oxide left on the copper surface in both cases.

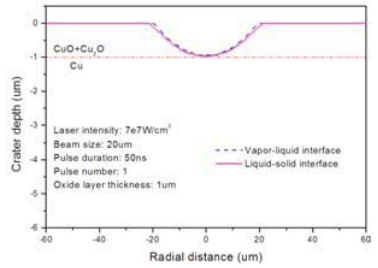

(a)

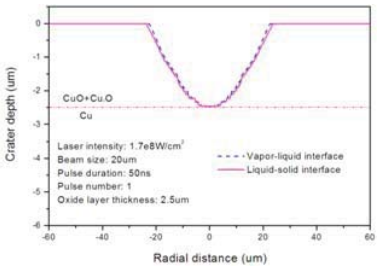

(b)

Fig. 6 Simulated craters generated by the model-determined intensity threshold (a) oxides layer thickness:1μm (b) oxides layer thickness:2.5μm

The 1-D heat conduction in semi-infinite solid model is traditionally used to model the laser ablative removal of oxides. The temperature at the surface is given by $T(0,t)=\frac{2I(1-Rl)}{K}(\sqrt{\frac{\alpha t}{\pi}})$, where I is the laser intensity, Rl is the surface reflectivity, K is heat conductivity, α is heat diffusivity. Suppose that the laser intensity heating the surface to the evaporation temperature at the end of the pulse (50ns in this case) is intensity threshold. Therefore, the CuO evaporation threshold of 8.24×10^6 W/cm^2 is regarded as the cleaning threshold.

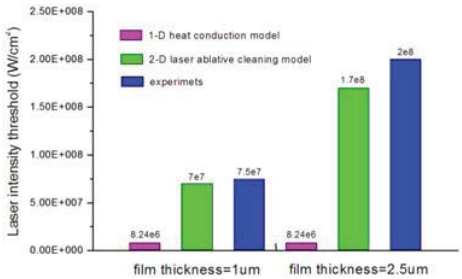

Fig. 7 Comparison of intensity thresholds determined by 1-D heat conduction model, 2-D laser ablative cleaning model and experiments

The thresholds determined by experiments, 1-D heat conduction model and 2-D laser ablative cleaning model are shown in Fig. 7. The 1-D model determined threshold is far below the experimentally determined thresholds, and unrelated to the oxide layer thickness. The thresholds determined by the 2-D model are very close to the experimental values. Clearly, this 2-D laser ablative cleaning model can more accurately estimate the threshold.

Multiple-pulse Irradiation Strategy

Using multiple-pulses with a lower intensity is an alternative to the single-pulse mode in that it offers easier control over damage avoidance to the substrate. But it takes a longer time and pulse repetition rate plays a role.

Effect of Laser Intensity The laser intensity under the multiple-pulse strategy should be higher than the evaporation threshold of CuO and lower than the melting threshold of Cu substrate. The former is determined as 1.19×10^7 W/cm^2 by the 2-D laser ablative cleaning model, and the latter is determined as 6.5×10^7 W/cm^2 by the 2-D laser ablation model in [19]. Hence, three laser intensity values of 1.25×10^7 W/cm^2, 3.0×10^7 W/cm^2 and 5.5×10^7 W/cm^2 are chosen for the following investigation.

Fig. 8 shows the experimental and simulated results of the variation of crater depth with the pulse number under different laser intensity levels. The experimental crater depth was measured using Atomic Force Microscopy (AFM). Please note that there are no experimental results of crater depth when the substrate is damaged. This is because the damaged substrate becomes so rough at the local area that AFM can not be used. In addition, for the intensity of 1.25×10^7 W/cm^2, only simulation results are shown.

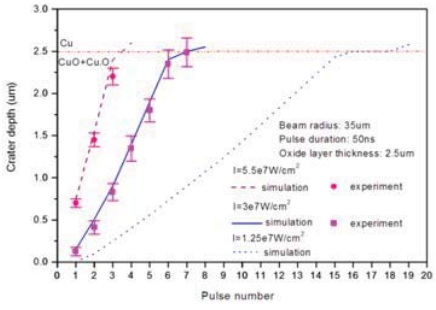

Fig. 8 Experiments and simulations of the crater depth increase with the pulse number under different laser intensity levels

With the intensity of 5.5×10^7 W/cm^2, 3 pulses can not completely remove the oxide film, and 4 pulses do damage the substrate. For the intensity of 3×10^7 W/cm^2, the crater produced by the 7th pulse ceases to deepen after the very thin oxide layer left by the 6th pulse is removed, and the 8th pulse makes the Cu surface start to melt. SEM images of the sample surfaces corresponding to the above mentioned four cases are shown in Fig. 9. The surface morphology is consistent with the results shown in Fig. 8. With the intensity of 1.25×10^7 W/cm^2, the oxide layer is completely removed after the irradiation of 15 pulses. However, the 16th, 17th and 18th pulses directly irradiating on the naked Cu substrate have no damage to Cu surface.

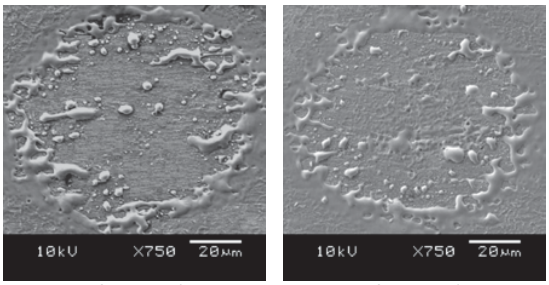

After 7 pulses After 8 pulses

(a)

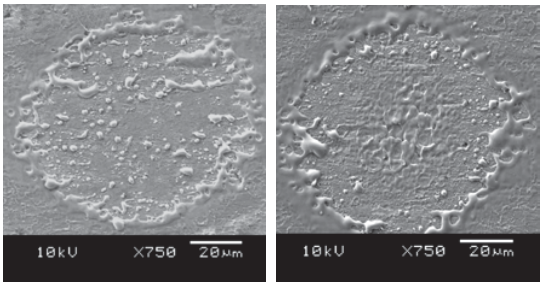

After 3 pulse After 4 pulses

(b)

Fig. 9 SEM images of copper cleaned by multiple-pulse having different laser intensity (a) 3×10^7W/cm^2 (b) 5.5×10^7W/cm^2

Fig. 10 shows the simulated peak temperature induced by different pulse number at the point on the copper substrate corresponding to the beam center. With the intensity of 1.25×10^7 W/cm^2, the peak temperature induced by 16, 17 and 18 pulses is below 1356 K, which confirms the existence of intact copper surface. It can be concluded that the excessive number of pulses with this rather low laser intensity will not damage the copper substrate. On the other hand, the peak temperature corresponding to the case of Cu surface melting goes beyond 1356 K, namely 4 pulses

with the intensity of 5.5×10^7 W/cm^2 and 8 pulses with the intensity of 3×10^7 W/cm^2.

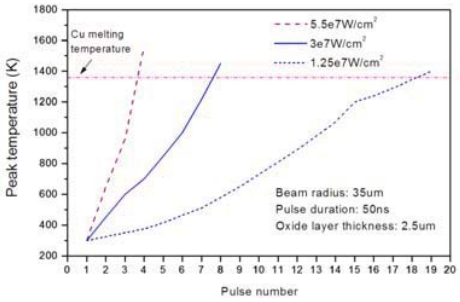

Fig. 10 Simulated peak temperature at the location corresponding to the beam center on the copper surface

The ablation rate is defined as the thickness of oxide layer removed by a pulse, equal to the depth of crater generated by a pulse. Fig. 11 shows the experimental and simulated ablation rate with different pulse number under two intensity levels. The ablation rate increases with the laser intensity rising, which agrees with the fact of less pulse number required under higher laser intensity shown in Fig. 8. In addition, with the identical laser intensity, the ablation rate also goes up with the pulse number. This is due to the continuous increase of heat accumulation with the pulse number. However, for the intensity of 3×10^7 W/cm^2, the ablation rate of the 7th pulse becomes smaller since this intensity is not sufficient high to damage the Cu substrate.

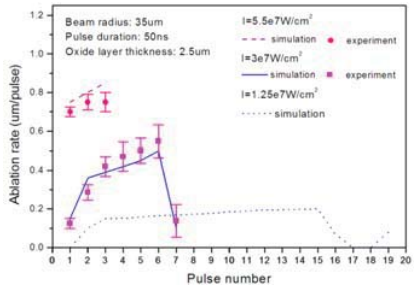

Fig. 11 Experimental and simulated ablation rate with the different pulse number and laser intensity

Most simulated ablation rates are higher than the corresponding experimental values due to the over-estimation of temperature in the simulation. However, the experimental ablation rates of the 3rd to the 6th pulse with the intensity of 3×10^7 W/cm^2 are higher than the simulated values possibly due to the involvement of the shock wave. The shock wave induced by the plasma gets stronger with the increase in pulse number.

Effect of Repetition Rate Fig. 12 shows the AFM measured craters produced by 4 pulses with the intensity of 3×10^7 W/cm^2 under the repetition rates of 1 kHz and 2 kHz, respectively. It is observed that the crater produced under 1 kHz is shallower and narrower than that under 2 kHz. The experimental and simulated results about the variation of crater depth with the pulse number under different repetition rates are presented in Fig. 13. The depth of 5 pulses produced

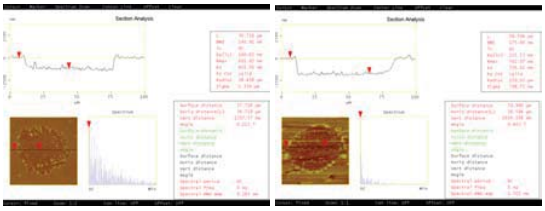

(a) (b)

Fig. 12 AFM measurements of the craters generated by four laser pulses with different repetition rates (a) 1 kHz (b) 2 kHz

crater under 2 kHz is roughly equal to that of 7 pulses produced crater under 1 kHz. Obviously, the less pulse number is required in the case of the high repetition rate. Fig. 14 shows the simulated crater generated by 5 pulses with laser intensity of 3×10^7 W/cm^2 under the repetition rate of 1 kHz and 2 kHz and the corresponding temperature distribution in the material, respectively. The simulated variation of the crate depth with the repetition rate is very similar to the experimentally obtained one shown in Fig. 11.

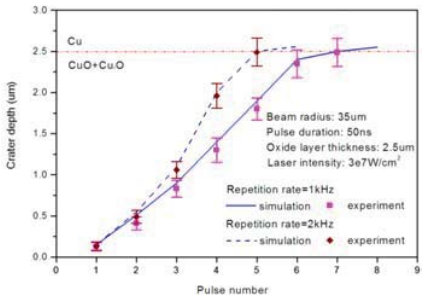

Fig. 13 Experimental and simulated crater depth increase with the pulse number under two repetition rates

Fig. 15 shows the simulated temperature history of the point on the Cu surface corresponding to the beam center. The pulse periods corresponding to the repetion rates of 1 kHz and 2 kHz are 1 ms and 0.5 ms, respectively. With the pulse period decreasing, the heat dissipating time between two consecutive laser pulses gets shorter and the temperature decreases less. Thus,

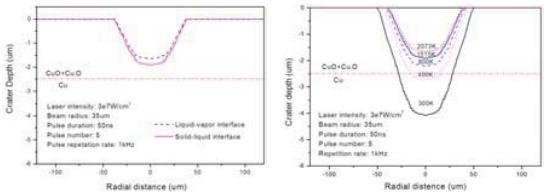

(a)

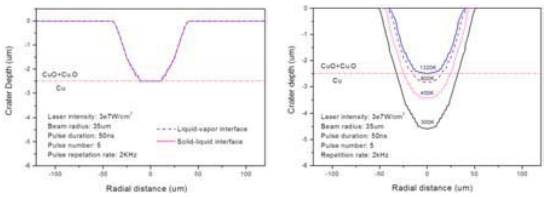

(b)

Fig. 14 Simulations of craters generated by five pulses and the corresponding isothermal contours in the material. (a) 1 kHz (b) 2 kHz

more heat is accumulated. This fact can be seen in Fig. 15. Due to the more severe heat accumulation in the case of 2 kHz, the temperature induced by the 5th pulse is significantly higher than that under 1 kHz. This is the reason that higher repetition rate can reduce the required pulse number to remove the oxides layer under the identical laser intensity.

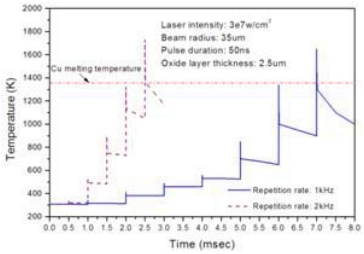

Fig. 15 Simulated temperature history at the location corresponding to the beam center on the Cu surface

Conclusions

Different oxide layer thickness values with CuO and Cu_2O distributions at the thickness direction are considered. The 2-dimensional laser ablative cleaning model has a two-layer structure and is used to comparatively study single-pulse and multiple-pulse irradiation strategies. Under the single-pulse strategy, the cleaning process can be completed with a single pulse while the intensity threshold not causing substrate damage is difficult to experimentally determine. This model can determine the intensity threshold with a safety margin not to damage the underlying substrate. Under the multiple-pulse strategy, it takes multiple pulses to remove an oxide layer without damaging the substrate while the laser intensity has a much larger window of operation. With a little lower laser intensity, it takes more pulses to remove the oxide but a few extra pulses will not damage the substrate and thus gives a larger safety margin. The higher the laser repetition rate, the fewer the laser pulse number is required by the safe cleaning.

Acknowledgement

The authors are grateful to Mr. Adrian M Chitu, Mr. Alex Wu and Mr. Shengguo Jia for their technical assistance during AFM, XPS and Ellipsometer measurements, respectively.

References

[1] Zapka, W., Ziemlich, W., and Tam, A.C. (1991) Efficient pulsed laser removal of 0.2 μm sized particles from a solid surface, Appl. Phys. Lett. **58**, 2217-2219.

[2] Zhou, X., Imasaki, K., Furukawa, H., Umino, H., Sakagishi, K., Nakai, S., and Yamanaka, C. (2001) Basic Study on Laser Ablation Surface Cleaning of Nuclear Facility, Surf. Engi., v **17**, n **5**, 384-388.

[3] Tam, A. C., Leung, W. P., Zapka, W., and Ziemlih, W. (1992) Laser-cleaning Techniques for Removal of Surface Particulates, J. Appl. Phys., **71(7)**, 3515-3523.

[4] Tsunemi, A., Hagiwara, K., Saito, N., Nagasaka, K., Miyamoto, Y., Suto, O., and Tashiro, H. (1996) Complete removal of paint from metal surface by ablation with a TEA CO_2 laser, Appl. Phys. A, **v63**, n5, 435-439.

[5] Meja, P., Autrie, M., Alloncle, P., Pasquet, P., Oltra, R., and Boquillon, J. P. (1999) Laser Cleaning of Oxidized Iron Samples: The Influence of Wavelength and Environment, Appl. Phys. A, **69**, 687-690.

[6] Solis, J., Vega, F., and Afonso, C. N. (1996) Kinetics of Laser-induced Surface Melting and Oxide Removal in Single-crystalline Ge, Appl. Phys. A., 62, 197-202.

[7] Lim, H., and Kim, D. (2004) Laser-assisted Chemical Cleaning for Oxide-scale Removal from Carbon Steel Surfaces, Journal of Laser Applications, **Vol. 16**, Number 1, 25-30.

[8] Steen, W. M. (1998) Laser Material Processing, Springer-Verlandag, London, pp. 327-350.

[9] Magyar, J., Sklyarov, A., Mikaylichenko, K., and

Yakovlev, V. (2003) Silicon Dioxide Thin Film Removal Using High-power Nanosecond Lasers, Appl. Surf. Sci., **207**, 306-313.

[10] Psyllaki, P., and Oltra, R. (2000) Preliminary Study on the Laser Cleaning of Stainless Steel after High Temperature Oxidation, Materials Science & Engineering, A**282**, 145-152.

[11] Wesner, D. A., Mertin, M., Lupp, F., and Kreutz, E. W. (1996) Cleaning of Copper Traces on Circuit Boards with Excimer Laser Radiation, Appl. Surf. Sci., **96-98**, 479-483.

[12] Yonezawa, Y., Minamikawa, T., Morimoto, A., and Shimizu, T. (1998) Removal of Surface Oxides on Copper by Pulsed Laser Irradiation, Jpn. J. Appl. Phys., **Vol. 37**, 4505-4509.

[13] Kearns, A., Fischer, C., Watkins, K. G., Glasmacher, M., Kheyrandish, H., Brown, A., Steen, W. M., and Beahan, P. (1998) Laser Removal of Oxides from a Copper Substrate Using Q-switched Nd:YAG Radiation at 1064nm, 532nm and 266nm, Appl. Surf. Sci., **127-129**, 773-780.

[14] Lee, J. M., Watkins, K. G., and Steen W. M. (2001) Characterization of Laser Cleaning of Copper for Soldering Processes, ASME J. Manuf. Sci. Eng., **23**, 521-527.

[15] Lee, S. K., Yoon, K. K., Whang, K. H., and Na, S. J. (1999) Excimer Laser Ablation removal of Thin Chromium films from Glass Substrates, Surf. Coat. Technol., **113**, 63-74.

[16] Azzam, R. M. A., and Bashara, N. M. (1977) Ellipsometry and polarized light, North-Holland Pub. Co., New York.

[17] Vickerman, J. C. (1997), Surface Analysis-The principal Techniques, JohnWiley&Sons Ltd, Chichester, England.

[18] Hauffe, K. (1965) Oxidation of Metals, Plenum Press, New York.

[19] Zhang, W. W., Yao, Y. L., and Chen, K. (2001) Modelling and Analysis of UV Laser Micromachining of Copper, Int. J. Adv. Manuf. Technol., **18**, 323-331.

[20] Samsonov, G. V. (1982) The Oxide Handbook, IFI/Plenum, New York.

[21] Grivoriev, I. S. and Meilikhov, E. Z. (1997) Handbook of Physical Quantities, CRC Press, New York.

[22] Duley, W. (1996) UV Lasers: Effects and Applications in Materials Science, Cambridge University Press, Cambridge.

[23] Palik, E. (1991) Handbook of Optical Constants of Solids II, Academic Press, San Diego, pp. 875-878.

[24] Meirmanov, A. M. (1992) The Stefan Problem, Walter de Gruyter, Berlin.

[25] Knight, C. J. (1979) Theoretical modeling of rapid surface vaporization with back pressure, AIAA Journal, **17**(5), 519-523.

[26] Voller, V. R. and Prakash, C. (1987) A fixed grid numerical modeling methodology for convection–diffusion mushy region phase-change problems, Int. J. of Heat Mass Transfer, **30**(8), 140-145.

[27] Chastain, J., and King, J. R. (1995) Handbook of X-ray Photoelectron spectroscopy, Physical Electronics, Inc., Eden Prairie.

[28] Haugsrud, R. (2002) The Influence of Water Vapor on the Oxidation of Copper at Intermediate Temperature, Journal of the electrochemical Society, **149**(1), B14-B21.

Meet the Authors

Jie Zhang is a Ph.D candidate in the Department of Mechanical Engineering at Columbia University. She received a BS in 1993 and a MS in 1997 in Mechanical Engineering from Xi'an Jiaotong University, China.
Youneng Wang is a Ph.D candidate at Columbia University. His research interests are laser shock peening, laser peen forming and laser micromachining.
Peng Cheng is a Ph.D candidate in the Department of Mechanical Engineering at Columbia University. He received a BS in 1997 and a MS in 2000 in Mechanical Engineering from Tsinghua University, China.
Y. Lawrence Yao is a Professor in the Department of Mechanical Engineering at Columbia University. He received his Ph.D. from the University of Wisconsin-Madison in 1988. He serves on the Board of Directors of LIA.